
VARIATIONAL QUANTUM POLICY GRADIENTS WITH AN APPLICATION TO QUANTUM CONTROL

A PREPRINT

 **André Sequeira**

Universidade do Minho, HASLab / INESC TEC, INL

Department of Informatics, Braga, Portugal

andresequeira401@gmail.com

 **Luís Paulo Santos**

Universidade do Minho, CSIG / INESC TEC, INL

Department of Informatics, Braga, Portugal

psantos@di.uminho.pt

 **Luís Soares Barbosa**

Universidade do Minho, HASLab / INESC TEC, INL

Department of Informatics, Braga, Portugal

1sb@di.uminho.pt

March 22, 2022

ABSTRACT

Quantum Machine Learning models are composed by VQC in a very natural way. There are already some empirical results proving that such models provide an advantage in supervised/unsupervised learning tasks. However, when applied to RL, less is known. In this work, we consider Policy Gradients using an hardware-efficient ansatz. We prove that the complexity of obtaining an ϵ -approximation of the gradient using quantum hardware scales only logarithmically with the number of parameters, considering the number of quantum circuits executions. We test the performance of such models in benchmarking environments and verify empirically that such quantum models outperform typical classical neural networks used in those environments, using a fraction of the number of parameters. Moreover, we propose the utilization of the Fisher Information spectrum to show that the quantum model is less prone to barren plateaus than its classical counterpart. As a different use case, we consider the application of such variational quantum models to the problem of quantum control and show its feasibility in the quantum-quantum domain.

Keywords Variational Quantum Circuits, Policy Gradients, Deep Reinforcement Learning

1 Introduction

RL is responsible for many important developments in Artificial Intelligence. Successes such as beating the world champion of Go [1] and being able to solve numerous complex games without any human intervention [2] were relevant milestones in Artificial Intelligence. For the first time, algorithms can capture the essence of complex environments and perform optimal planning without any supervising. Indeed, RL became useful in real-world complex problems such as self-driving vehicles [3], automated trading [4, 5], recommender systems [6] and quantum physics [7], among many others. The recent advancements in RL are strongly associated to advances in Deep Learning [8]; RL models based on deep neural networks enable scaling to environments with large state-action spaces.

There are already some results suggesting that RL agents obeying quantum mechanics rules can outperform classical RL agents [9, 10, 11, 12, 13] and were even tested in a real photonic quantum device [14]. Although provable quantum speedups have been shown, these algorithms suffer from the same scaling problem as classical RL tabular methods [15]: they do not scale easily to real-world problems with large state-action spaces. Additionally, the lack of fault-tolerant quantum computers [16] further compromises the ability to robustly execute algorithms handling problems of significant size.

VQC present themselves as viable alternatives to the algorithms reported in the references above. Besides being shallow enough to be confidently executed on current NISQ (*Noisy Intermediate Scale Quantum*) hardware [17], they are parameterized models able to learn the task at hand. Variational models are also referred to as quantum neural networks [18]. Although approximately universal [19], fundamental questions on the expressivity and trainability of VQC remain to be answered, especially from a perspective relevant to RL.

This paper proposes the use of VQC to construct policies for RL agents, leading to a quantum version of the Policy Gradient algorithm [20]. Their effectiveness is shown through some well known benchmarking environments, empirically demonstrating an advantage with respect to classical neural networks from both a scoring perspective and in what concerns the size of the network, i.e. the total number of parameters to optimize. It is proved that gradient estimation, using quantum hardware, exhibits a logarithmic complexity with the number of parameters to be optimized. Furthermore, it is empirically demonstrated that randomly initializing the parameters of the quantum neural network can vastly damage the agent's performance suggesting that there is an optimal initialization strategy for policy gradients in benchmarking environments. The effect of barren plateaus in policy gradients, compared with classical neural networks, is studied using the Fisher information matrix spectrum as a metric. Finally, as a first step towards applying variational quantum models in the quantum-quantum domain, we suggest an application to quantum control where the quantum agent learns how to prepare a single-qubit gate with high fidelity in a model-free scenario, i.e. without any notion of the system's hamiltonian. In optimal quantum control, gate fidelity is improved by exploiting the full knowledge of the system's Hamiltonian [21]. However, when the system's dynamics is unknown, such methods are no longer viable. This constitutes the reason why applying the variational quantum methods may indeed be relevant [22]. In this setting, a quantum RL agent optimize in a model-free setting the gate fidelity, learning from the noisy environment.

The main contributions of this paper are:

- development of softmax-policies using shallow VQC showing an empirical advantage in benchmarking environments in terms of the average cumulative reward, compared to classical neural networks.
- reduction in the total number of parameters trained compared to classical neural networks and other quantum models applied to the same benchmarking environments.
- remonstration of a logarithmic bound on the gradient estimation sample complexity with respect to the number of parameters.
- development of an initialization technique for quantum policy gradients.
- study of barren plateaus in quantum policy gradient optimization surface for benchmarking environments, using the Fisher Information matrix spectrum as a metric.
- design of a quantum control environment application as a use case for the variational quantum model.

The rest of the paper is organized as follows. Section 2 reviews the state-of-the-art of quantum variational methods applied to RL with function approximation. Section 3 summarizes the fundamental theory behind Policy Gradient methods. Section 4 details the design of the proposed VQC and the correspondent quantum variational policy gradient algorithm. Section 5 explores trainability under gradient-based optimization using quantum hardware and estimates the number of samples needed to approximate the gradient. Section 6 presents the performance of the quantum variational algorithm on benchmarking environments. Moreover, an empirical analysis comparing the quantum and classical algorithms is given. Section 7 presents the benefits of using VQC from a theoretical basis, supporting the empirical advantage shown in the previous section. In Section 8 we explore the applicability of the proposed variational quantum circuit in the context of a quantum-quantum setting, by designing a quantum control environment. Section 9 closes the paper with some concluding remarks and suggestions for future work.

2 Related Work

Despite numerous publications focusing on Quantum Machine Learning (QML), the literature on variational methods applied to Reinforcement Learning (RL) remains scarce. Most results to date focus on value-based function approximation rather than policy-based. Chen et al. [23] use Variational Quantum Circuits (VQC's) as quantum value function approximators for discrete state-spaces and, in [24] the authors generalize the former result to continuous state-spaces. Even if the above methods exhibit promising results in a range of problems, Lockwood et al. [25] show that simple Q-Networks (i.e. state-action value approximators) based on Double Deep Q-Learning are not adequate for some environments, such as the Pong and Breakout Atari games. Indeed, there are environments in which Policy-based methods, which learn a policy instead of a value function, promise to achieve better performance.

Jerbi et al. [26] proposes a novel quantum variational policy-based algorithm achieving better performance than previous value-based methods in a set of benchmarking environments. Our work uses an *hardware-efficient ansatz* to construct a simpler variational architecture that solves well-known benchmarking environments. It exploits different initialization techniques and uses a different methodology to analyse the impact of classical and quantum policies applied to Policy Gradient methods.

Sanches et al. [27] also show promising results applying hybrid quantum-classical policy-based algorithms to solve real-world problems like vehicle routing. In [28], the authors propose a variational method for the Actor-Critic framework of RL, with both actor and critic being represented as VQC's; this is the only work so far operating on the quantum-quantum context of QML [29], i.e. a quantum agent acting upon a quantum environment. The authors suggest that the variational method could be used to solve quantum control problems. Our approach is to consider the simpler policy-based algorithm REINFORCE, to derive a policy for quantum control problems.

3 Policy Gradient methods

Differently from value-based methods, Policy Gradient methods try to learn a parameterized policy $\pi(a|s, \theta) = \Pr\{a_t = a|s_t = s, \theta_t = \theta\}$, where $\theta \in \mathbb{R}^k$ is the parameter vector of size k , s and a are the state and action, respectively, and t is the time instant, that can optimally select actions without resorting to a value function. These methods try to maximize a performance measure $J(\theta)$, also referred to as objective function, by performing gradient ascent on $J(\theta)$, i.e.

$$\theta_{i+1} = \theta_i + \eta \nabla_{\theta_i} J(\theta_i) \quad (1)$$

where η is the learning rate. The policy is parameterized either by a linear function or an Artificial Neural Network (ANN's). Provided that the action space is discrete and relatively small, then the most prominent way of balancing exploration and exploitation is by sampling an action from the so-called *Softmax-Policy*, also known as Neural Policy [30]:

$$\pi(a|s, \theta) = \frac{e^{h(s, a, \theta)}}{\sum_{b \in A} e^{h(s, b, \theta)}} \quad (2)$$

where $h(s, a, \theta) \in \mathbb{R}$ is a numerical preference for each state-action pair and A is the action set. For the sake of legibility, A will be omitted whenever a policy similar to equation (2) is presented. The policy gradient theorem [31] states that the gradient of the objective function can be casted as a function of the policy itself as in Equation (3):

$$\nabla_{\theta} J(\theta) = \mathbb{E}_{\pi} [R_{sa} \nabla_{\theta} \log \pi(a|s, \theta)] \quad (3)$$

where R_{sa} is the reward obtained from starting in state s and taking action a .¹ Equation (6) refers to a single time-step gradient. In general, the Monte-Carlo policy gradient known as REINFORCE [20], computes the gradient of samples obtained from N trajectories of length T (i.e. sequences of T actions) under the parameterized policy. Therefore, the reward R_{sa} is replaced by the correspondent γ -discounted cumulative reward, known as the *return* and denoted by $G(\tau)$ (see Equation (4)), for trajectory τ . The return from each time step t of the trajectory is calculated as in Equation (5):

$$G(\tau) = \sum_{t=0}^{T-1} \gamma^t r_{t+1} \quad (4)$$

$$G_t(\tau) = \sum_{t'=0}^{T-1} \gamma^{t'} r_{t'+t} \quad (5)$$

leading to the following policy-gradient update rule:

$$\nabla_{\theta} J(\theta) = \mathbb{E}_{\tau \sim \pi_{\theta}} \left[\sum_{t=0}^{T-1} G_t(\tau) \nabla_{\theta} \log \pi(a_t|s_t, \theta) \right] \quad (6)$$

A known limitation of the REINFORCE algorithm happens due to Monte-Carlo estimates. Stochastically sampling the trajectories results in gradient estimators with high variance, which deteriorate the performance as the environment's complexity increases [32]. Therefore, a variance reduction technique known as control variate or *baselines* $b(s_t)$ is used to improve the Monte Carlo gradient estimator without increasing the number of samples N . Baselines are subtracted

¹It is important to refer that Equations (3) and (6) assume the same initial state, thus ignoring the expectation over the initial state distribution, d_0 . The general expression should have $\mathbb{E}_{d_0, \pi}$

to the return such that it smooths the optimization landscape. Algorithm 1 presents REINFORCE with baseline, which estimates the gradient at each time step with a batch size of N trajectories. For the benchmarking environments in Section 6, we use the average return as the variance reduction baseline, calculated as in equation (7).

$$b(s_t) = \frac{1}{T-t} G_t(\tau) \quad (7)$$

Algorithm 1: REINFORCE with baseline

Data: Parameterized policy π_θ , learning rate η

while *True* **do**

- $\nabla_\theta J(\theta) = 0$;
- for** $i = 0 \dots N - 1$ **do**

 - Generate trajectory of the form $\tau_i = \{(s_0, a_0, r_0), \dots, (s_{T-1}, a_{T-1}, r_{T-1})\}$ following π_θ
 - Compute gradient with baseline $\nabla_\theta J(\theta) = \nabla_\theta J(\theta) + \sum_{t=0}^{T-1} (G_t(\tau_i) - b(s_t)) \nabla_\theta \log \pi(a_t | s_t, \theta)$

- end**
- $\nabla_\theta J(\theta) = \frac{1}{N} \nabla_\theta J(\theta)$
- update parameters via gradient ascent $\theta = \theta + \eta \nabla_\theta J(\theta)$

end

Advanced Policy-Gradient methods, like Actor-Critic [33], are known to further reduce the variance of the gradient estimate, however, with a cost of an additional value-function approximator.

4 Quantum Policy Gradient methods

This section details the VQC-based policy gradient proposed here. The main difference with respect to classical neural policies is that numerical preferences $h(s, a, \theta) \in \mathbb{R}$ are the output of measurements in a given parameterized quantum circuit. The result can be represented as the expectation value of a given observable or the probability of measuring a basis state. We resort to the former, since it allows for more compact representations of objective functions [34]. Additionally, the type of ansatz used by the proposed VQC implies that $\theta \in \mathbb{R}^k$ is a high dimensional vector corresponding to the angles of arbitrary single-qubit rotations.

VQC's are composed of four main building blocks, as represented in Figure 1. Initially, a state preparation routine or *embedding*, S , encodes datapoints into the quantum system. Next, a unitary $U(\theta)$ maps the data into higher dimensions of the Hilbert space. Such a parameterized model corresponds to linear methods in quantum feature spaces. This is followed by a measurement scheme, which obtains expectation values that are post-processed by a classical computer and fed to the objective function. We proceed by a careful analysis of each block of Figure 1 defining the full Quantum Neural Policy and a description of the correspondent training procedure.

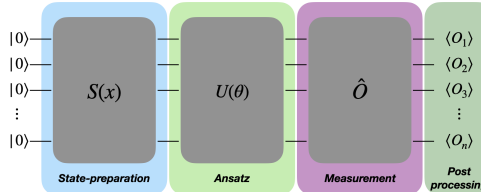


Figure 1: Building blocks of Variational Quantum Circuits.

4.1 Embedding

While classically there is no great emphasis on the encoding itself, the state-preparation routine is a crucial step for any variational quantum algorithms. Actually, there are numerous ways of encoding data into a quantum processor [35]. In order to allow for continuous-state spaces, angle encoding [36] is used. Arbitrary Pauli rotations $\sigma \in \{\sigma_x, \sigma_y, \sigma_z\}$ can

be used to encode a single feature per qubit. Hereby, given a state s with n features, $s = \{s_1, s_2, \dots, s_n\}$, σ_x rotations are used, requiring n qubits to encode $|s\rangle$, as given by equation (8):

$$|s\rangle = \bigotimes_{i=1}^n e^{-j\sigma_x s_i} |b_i\rangle \quad (8)$$

where $|b_i\rangle$ refers to the i th qubit of an n -qubit register initially in the zero state $|0^n\rangle$, i.e. $|b_i\rangle = |0\rangle$, for all i .

Each feature needs to be normalized such that $s_i \in [-\pi, \pi]$. Typically, in RL environments, the range of each feature is unknown. In this work, resorts to normalization based on the L_∞ norm. The main advantage of angle encoding lies in the simplicity of generating the encoding, given the composition of solely n single-qubit gates, thus giving rise to a circuit of depth 1. In contrast, the main disadvantage is the linear dependence between the number of qubits and the number of features characterizing the agent's state.

4.2 Parameterized model

In RL applications, unlike other domains, no *problem-inspired* ansatze which exploit the physics behind the problem are known, to the best of one's knowledge. This can be explained by the difficulty of expressing and training RL agent's policies as Hamiltonian-based evolution models [34]. Our goal however is to design a NISQ ansatz to capture the agent's optimal policy in different environments. Therefore, this work uses a parameterized model from the family of *hardware-efficient* ansatze [34] that has an adaptive behaviour as a classical feed-forward neural network. The main advantage of the hardware efficient ansatz is its versatility, accommodating encoding symmetries and bringing correlated qubits closer for depth reduction [37]. The ansatz consists of an alternating-layered architecture composed of single-qubit gates followed by a cascade of entangling gates as pictured in Figure 2.

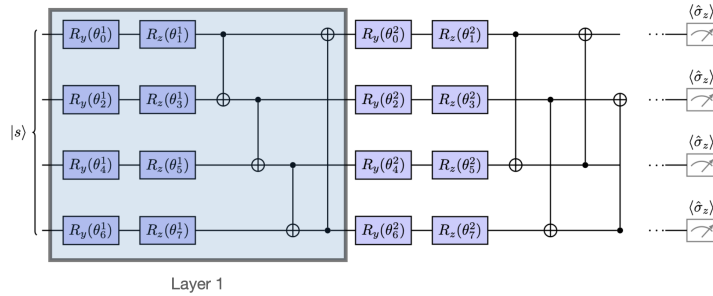


Figure 2: Hardware-efficient ansatz for RL based on single-qubit R_y, R_z rotation gates.

A single layer is composed of two single-qubit σ_y, σ_z rotation gates per qubit, i.e. applied to each angle encoded feature, followed by a cascade of entangling gates, such that features are correlated in a highly entangled state. The ansatz includes $2n$ single qubit rotation gates per layer, each gate parameterized by a given angle. Therefore, there are $2nL$ trainable parameters, for L total number of layers. The entangling gates follow a pattern that changes over the number of layers, inspired by the circuit-centric classifier design [19]. The pattern follows a modular arithmetic $\text{CNOT}[i, (i + l) \bmod n]$ where $i \in [1, \dots, n]$ and $l \in [1, \dots, L]$ indexes the layers. Increasing the number of layers increases the correlation between features.

4.3 Measurement

An arbitrary state $|\psi\rangle \in \mathbb{C}^{2^n}$ is represented by an arbitrary superposition over the basis states, as in Equation (9).

$$|\psi\rangle = \sum_{i=0}^{2^n-1} c_i |\psi_i\rangle \quad (9)$$

Measuring the state $|\psi\rangle$ in the computational basis (σ_z basis) collapses the superposition into one of the basis states $|\psi_i\rangle$ with probability $|c_i|^2$, as given by the Born rule [38]. In general, the expectation value of some observable \hat{O} , is

given by the summation of each possible outcome, i.e. the eigenvalue e_i weighted by its respective probability $|c_i|^2$ as in Equation (10).

$$\langle \hat{O} \rangle = \langle \psi | \hat{O} | \psi \rangle = \sum_{i=0}^{2^n-1} e_i |c_i|^2 \quad (10)$$

Let \hat{O} be the single-qubit σ_z^i measurement, applied to the i^{th} -qubit. Given that the σ_z eigenvalues are $[-1, 1]$, the expectation value $\langle \sigma_z^i \rangle$ can be obtained by Equation (11).

$$\langle \sigma_z^i \rangle = \langle \psi | \sigma_z^i | \psi \rangle = \sum_{i=0}^{2^n-1} (-1)^{f(i)} |c_i|^2 \quad (11)$$

where $f(i) = 1$ if the i^{th} -qubit is in the state $|1\rangle$, and $f(i) = 0$ otherwise. Note that estimating the expectation value depends on the knowledge about the probability of each outcome. For that reason, several circuit repetitions are required to obtain an accurate estimate of the expectation value. Let the state $|\psi\rangle$ be the quantum state obtained from the encoding of an agent's state via $S(s)$, and the parameterized block $U(\theta)$, as in Sections 4.1 and 4.2 respectively. Let $\langle \sigma_z^i \rangle$ be the quantum analogue of the numerical preference for action i , that we represent by $\langle a_i \rangle$ for clarity. Its expectation can be formally described by Equation (12) and estimated via Equation (11).

$$\langle a_i \rangle_\theta = \langle 0^n | S(s)^\dagger U(\theta)^\dagger \sigma_z^i U(\theta) S(s) | 0^n \rangle \quad (12)$$

For a policy with $|A|$ possible actions, each σ_z measurement corresponds to the numerical preference of each action, thus $|A|$ single-qubit estimated expectation values are needed. If the number of features in the agent's state is larger than the number of actions, the single-qubit measurements occur only on a subset of qubits. Such measurement scheme is qubit-efficient [35].

Figure 3 represents the full VQC for an environment with four feature states and four actions with three parameterized layers.

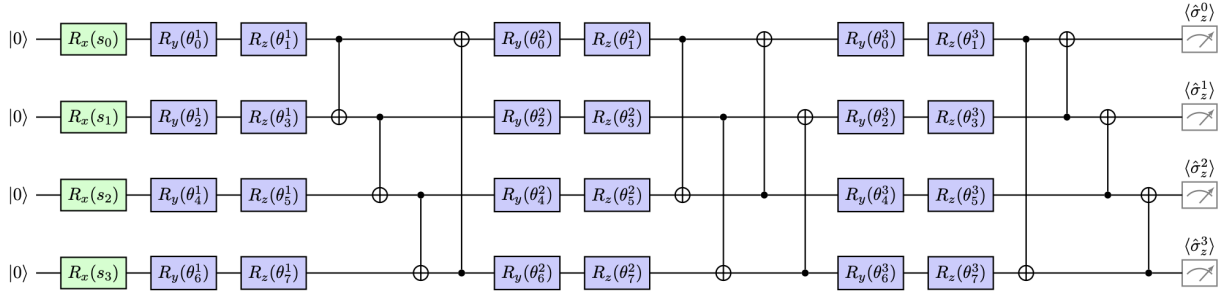


Figure 3: Variational Quantum Circuit for Policy-based RL with 3 parameterized layers.

4.4 Classical Post-processing

The final layer of the VQC, indicated in Figure 1 is the classical post-processing of the measurement outcomes. The goal of such post-processing is the conversion of estimated values to the quantum neural policy represented in Equation (13). The main difference compared to the softmax-policy of Equation 2 is that the numerical preference $h(s, a, \theta)$ is given by the expected values measured on the quantum processor, as calculated in Section 4.3.

$$\pi(a|s, \theta) = \frac{e^{\langle a \rangle_\theta}}{\sum_b e^{\langle b \rangle_\theta}} \quad (13)$$

Using a single σ_z measurement outcome to represent the numerical preference of one action as in Section 4.3, imposes a threshold upon the greediness of the ultimate policy generated. This will always allow for exploratory behaviour,

which can negatively impact on the performance of RL agents, especially in deterministic environments. As an example, consider the case of a 2-action MDP. The policy is a vector of two entries that represents a discrete probability distribution over the action set:

$$\pi = [\pi(a_0|s, \theta), \pi(a_1|s, \theta)] \quad (14)$$

Given that each entry of Equation (14) is given by a σ_z measurement, this value will be bounded to $\sigma_z \in [-1, 1]$. Therefore, the biggest difference between action preferences happens when the estimated vector is $[1, -1]$. Thus, the softmax normalized vector will be:

$$\pi_a = [\pi(a_0|s, \theta), \pi(a_1|s, \theta)] \quad (15)$$

$$= [0.88, 0.12] \quad (16)$$

In this case, the policy always has a ~ 0.1 probability of selecting the worst action; the same *rationale* applies to larger action sets. A trainable parameter β is added to the quantum neural policy as depicted by Equation (17). β has the effect of scaling the output values from the quantum circuit measurements. Such technique resembles an energy-based model, but instead of decreasing β over time, we consider it as a hyperparameter to be tuned along with θ and let the optimization itself find the optimal parameter that assures convergence towards the optimal policy, according to the necessities of the corresponding stochastic environment.

$$\pi(a|s, \theta) = \frac{e^{\beta \langle a \rangle_\theta}}{\sum_b e^{\beta \langle b \rangle_\theta}} \quad (17)$$

5 Gradient Estimation

Typically, classical optimization is used within the VQC's context to minimize/maximize the cost function. Although quantum-aware gradient-free optimizers already exist [39], this work resorts to classical gradient-based optimization is used, for two main reasons:

1. Gradient-based optimization provides significant advantages over gradient-free approaches, especially from the convergence point of view [40];
2. Gradient-based optimization can be performed using the same quantum device that computes expectations $\langle a_i \rangle_\theta$.

Gradient-based optimization on a quantum computer can be devised using *parameter-shift rules* [41], whose analytical formulation is presented in Equation (18).

$$\nabla_{\theta_i} \langle a_i \rangle_\theta = r_i \langle a_i \rangle_{\theta + \frac{\pi}{4r_i}} - r_i \langle a_i \rangle_{\theta - \frac{\pi}{4r_i}} \quad (18)$$

For parameterized models with single-qubit rotation gates in $\frac{1}{2}\{\sigma_x, \sigma_y, \sigma_z\}$ there are two distinct eigenvalues $r_i = \pm \frac{1}{2}$ (e.g. the model proposed in figure 2). The expectation values $\langle a_i \rangle_\theta$ are thus differentiable. This section analyses the number of samples necessary to obtain an ϵ -approximation of the policy-gradient (Equation (6)) using parameter-shift differentiation. The accuracy of the gradient is intrinsically dependent on the accuracy of the computed expectation values. Thus, a good estimate for the number of samples depends on the number of the quantum circuit evaluations.

Lemmas 5.1 - 5.6 are used to bound an unbiased estimate of the policy-gradient of a single trajectory presented in Equation (6). Notwithstanding, Algorithm 1 computes N estimates to further reduce the variance and increase the accuracy of the policy-gradient. For that reason, assuming N trajectories of T time-steps, the policy-gradient algorithm uses $\mathcal{O}(NT)$ samples. Theorem 5.7 bounds the optimal number of trajectories N , to achieve an ϵ -approximation of the policy-gradient.

Lemma 5.1 (ϵ -approximation of expectation value). *Let $\langle a_i \rangle_\theta$ be the numerical preference for action i obtained from the expectation value of the computational basis measurement. Let ϵ be the estimation associated error depending on the number of evaluations of the quantum circuit, m . An ϵ -approximation of the expectation value is:*

$$\langle a_i \rangle_\theta \in [-(1-\epsilon), 1-\epsilon] \quad (19)$$

$$\text{where } \epsilon = \sqrt{z \frac{\hat{p}(1-\hat{p})}{m}} \quad (20)$$

Proof. Measuring a single qubit is equivalent to sampling from a Bernoulli distribution. Therefore, the probability of a single-qubit to be bounded by Wald interval [35] with an error ϵ is

$$\epsilon = \sqrt{z \frac{\hat{p}(1-\hat{p})}{m}} \quad (21)$$

where z is the confidence level, \hat{p} is the estimate and m is the number of circuit repetitions. Equation (21) is maximized for $\hat{p} = \frac{1}{2}$ for the case of a uniform superposition. Given that the ideal single-qubit computational basis expected value is $\langle a_i \rangle_\theta \in [-1, 1]$, for approximation error ϵ , the ϵ -approximation is $\langle a_i \rangle_\theta \in [-(1-\epsilon), 1-\epsilon]$. \square

Lemma 5.2 (Range of the gradient of σ_z observable). *Let $\langle a \rangle_\theta$ correspond to the expectation value of a single-qubit computational basis measurement. The gradient of the observable using the parameter-shift rule (Equation (18)) is such that*

$$\nabla_\theta \langle a \rangle_\theta \in [-(1-\epsilon), 1-\epsilon] \quad (22)$$

Proof.

$$\nabla_\theta \langle a \rangle_\theta = r_i \langle a_i \rangle_{\theta+\frac{\pi}{4r_i}} - r_i \langle a_i \rangle_{\theta-\frac{\pi}{4r_i}} = \frac{1}{2} \left[\langle a_i \rangle_{\theta+\frac{\pi}{4r_i}} - \langle a_i \rangle_{\theta-\frac{\pi}{4r_i}} \right] \quad (23)$$

\square

and therefore belongs to the interval $[-(1-\epsilon), 1-\epsilon]$. Using parameter-shift rules in the context of policy gradients is not trivial, given the need to differentiate the neural policy in Equation (17), which cannot directly apply the parameter-shift rule to the expected values. However, expanding Equation (18) leads to a new expression for the gradient of the log-policy that depends intrinsically on expected values.

Lemma 5.3 (Log-policy gradient). *Let $\pi(a|s, \theta)$ be a policy s.t $\theta \in \mathbb{R}^k$ and $s \in S$, $a \in A$. Then, the log-policy gradient is given by the expansion in terms of the expectation values $\langle a_i \rangle_\theta$, estimated in a quantum circuit as*

$$\nabla_\theta \log \pi(a|s, \theta) = \beta \left(\nabla_\theta \langle a \rangle_\theta - \sum_b \pi(b|s, \theta) \nabla_\theta \langle b \rangle_\theta \right) \quad (24)$$

Proof.

$$\begin{aligned} \nabla_\theta \log \pi(a|s, \theta) &= \nabla_\theta \log \frac{e^{\beta \langle a \rangle_\theta}}{\sum_b e^{\beta \langle b \rangle_\theta}} \\ &= \nabla_\theta \left(\log e^{\beta \langle a \rangle_\theta} - \log \sum_b e^{\beta \langle b \rangle_\theta} \right) \\ &= \beta \nabla_\theta \langle a \rangle_\theta - \frac{\nabla_\theta \sum_b e^{\beta \langle b \rangle_\theta}}{\sum_b e^{\beta \langle b \rangle_\theta}} \\ &= \beta \left(\nabla_\theta \langle a \rangle_\theta - \sum_b \pi(b|s, \theta) \nabla_\theta \langle b \rangle_\theta \right) \end{aligned}$$

\square

Using Lemma 5.2 and Lemma 5.3, it is possible to bound the size of log-policy gradient.

Lemma 5.4 (Range of the log-policy gradient). *Let $\pi(a|s, \theta)$ be a policy s.t $\theta \in \mathbb{R}^k$ and $s, a \in S, A$. Then, the log-policy gradient is given by the gradient of observables $\langle a_i \rangle_\theta$. Thus, the log-policy gradient is bounded by*

$$\nabla_\theta \log \pi(a|s, \theta) = [-2\beta(1-\epsilon), 2\beta(1-\epsilon)] \quad (25)$$

Proof.

$$\nabla_\theta \log \pi(a|s, \theta) = \beta \left(\nabla_\theta \langle a \rangle_\theta - \sum_b \pi(b|s, \theta) \nabla_\theta \langle b \rangle_\theta \right) \quad (26)$$

□

which belongs to the interval $[-2\beta(1-\epsilon), 2\beta(1-\epsilon)]$. The last step required to obtain an unbiased estimate of the policy-gradient is to bound the return the agent can obtain following an arbitrary policy.

Lemma 5.5 (Return size). *Let R_{max} be the maximum reward the agent can obtain in a single time step t and $\gamma \in [0, 1]$ be the discount factor. Thus, the time-step return in Equation (6) is bounded by:*

$$G_t(\tau) = \frac{R_{max}}{1-\gamma} \quad (27)$$

Proof.

$$G_t(\tau) = \sum_{t=0}^{\infty} \gamma^t r_t \leq \sum_{t=0}^{\infty} \gamma^t R_{max} \leq R_{max} \sum_{t=0}^{\infty} \gamma^t \leq \frac{R_{max}}{1-\gamma} \quad (28)$$

□

Using Lemma 5.5 and Lemma 5.4, it is possible to bound an unbiased estimate of the policy-gradient.

Lemma 5.6 (unbiased estimate of the policy-gradient). *Let τ be a trajectory sampled under policy π . Thus, for T steps, an unbiased estimate of the gradient is bounded by:*

$$\nabla_\theta J(\theta) \in \left[-2\beta(1-\epsilon)T \frac{R_{max}}{1-\gamma}, 2\beta(1-\epsilon)T \frac{R_{max}}{1-\gamma} \right] \quad (29)$$

Proof.

$$\begin{aligned} \nabla_\theta J(\theta) &= \mathbb{E}_{\tau \sim \pi_\theta} \left[\sum_{t=0}^{T-1} G_t(\tau) \nabla_\theta \log \pi(a_t|s_t, \theta) \right] \\ &\leq \frac{R_{max}}{1-\gamma} \mathbb{E}_{\tau \sim \pi_\theta} \left[\sum_{t=0}^{T-1} \nabla_\theta \log \pi(a_t|s_t, \theta) \right] \\ &\leq \frac{R_{max}}{1-\gamma} \sum_{t=0}^{T-1} [\mathbb{E}_{\tau \sim \pi_\theta} \nabla_\theta \log \pi(a_t|s_t, \theta)] \\ &\leq \frac{R_{max}}{1-\gamma} T [\mathbb{E}_{\tau \sim \pi_\theta} \nabla_\theta \log \pi(a_t|s_t, \theta)] \end{aligned} \quad (30)$$

□

which belongs to the interval $[-2\beta(1-\epsilon) \frac{R_{max}}{1-\gamma} T, 2\beta(1-\epsilon) \frac{R_{max}}{1-\gamma} T]$. Lemma 5.6 bounds the size of an unbiased estimate of the policy-gradient in a single episode of T steps. Considering N different estimates, the agent requires $\mathcal{O}(NT)$ samples. Let $\nabla_k J(\theta)$ be the k^{th} component of the gradient, Theorem 5.7 provides a bound on the number of samples required to obtain an ϵ -approximation, concerning all parameters k .

Theorem 5.7 (ϵ -approximation of the policy-gradient). *Let $\theta \in \mathbb{R}^k$. In order to generate, with probability $1 - \delta$, an ϵ -approximate estimate $\nabla_\theta J(\theta)$ such that*

$$|\nabla_\theta^* J(\theta) - \nabla_\theta J(\theta)| \leq \epsilon \quad (31)$$

the quantum policy-gradient requires a number of samples given by:

$$\mathcal{O}(NT) = \frac{8T^3(\frac{R_{max}}{1-\gamma})^2 \beta^2 (1-\epsilon)^2}{\epsilon^2} \log(\frac{k}{\delta}) \quad (32)$$

Proof. Consider the bound on the unbiased estimate of the policy-gradient (Lemma 5.6). From Hoeffding's inequality [42], an average gradient of N estimates is ϵ -approximate with probability given by Equation (33)

$$\mathbb{P} [\nabla_{\theta}^* J(\theta) - \nabla_{\theta} J(\theta) \geq \epsilon] \leq \exp \left(-\frac{2N\epsilon^2}{(4\beta(1-\epsilon)T\frac{R_{max}}{1-\gamma})^2} \right) \quad (33)$$

From the union bound, for all parameters k , the probability is less than

$$\mathbb{P} \left[\bigcup_{i=1}^k \exp \left(-\frac{2N\epsilon^2}{(4\beta(1-\epsilon)T\frac{R_{max}}{1-\gamma})^2} \right) \right] \leq k \exp \left(-\frac{2N\epsilon^2}{(4\beta(1-\epsilon)T\frac{R_{max}}{1-\gamma})^2} \right) \quad (34)$$

Let δ be the probability computed by the Equation (34). Hence, if

$$N = \frac{8T^2(\frac{R_{max}}{1-\gamma})^2\beta^2(1-\epsilon)^2}{\epsilon^2} \log\left(\frac{k}{\delta}\right) \quad (35)$$

the gradient estimate is ϵ -approximately correct, with probability $1 - \delta$. Moreover, ϵ reflects the approximation error inherited from sampling single-qubit measurements. In addition, an ϵ -estimate of the gradient scales only logarithmically with the number of parameters. \square

6 Performance in simulated environments

This section discusses the performance of the proposed quantum neural policy through evaluation with well known benchmarking environments from the OpenAI Gym library [43]. Empirical evidence is shown that the quantum neural policy can outperform typical classical neural networks used in several toy problems. The following performance assessment methodology was used:

1. several classical neural policies, composed of classical neural networks with two hidden layers, were used and the best performing network was selected;
2. the performance of the best classical neural policy was compared with the quantum model using the empirical reward over the number of episodes as the figure of merit.

All quantum circuits were built using the Pennylane library [44] and trained using the PyTorch automatic differentiation backend [45]. All training instances used the most common classical optimizer, ADAM [46].

6.1 Numerical Experiments

The CartPole-v0 and Acrobot-v1 environments were selected as benchmarks for the quantum neural policy. They have a continuous state-space with a relatively small feature-space (2 to 6 features). Moreover, they share a small discrete action-space (2 to 3 possible actions). The reward function varies accordingly to each environment, making it harder to learn from environment to environment. For example, the CartPole environment is known to have a high variance. Environments have different episode lengths as well. All environment specifications are presented in table 1.

Environment	#Features	#Actions	Reward Function (per step)	Max #steps (per episode)	Terminal states
CartPole-v0	4	2	1	200	Out of bounds or reward 200 or below horizontal line
Acrobot-v1	6	3	-1	500	500 steps

Table 1: Description of the environments.

Figures 4 and 5 present the average reward for different classical network configurations for the benchmarking environments. The results show that a fully connected neural network with two hidden layers of 64 neurons each performs reasonably better than other architectures for the CartPole-v0 environment. For Acrobot-v1 the fully connected neural network with a hidden-layer of 64 neurons and 128 neurons behave similarly. However, as the plot depicts, the network with 64 neurons has a stable training which justifies its choice. During training, the agent's performance was substantially damaged using other architectures, reflected in the sharp curve in the picture. Such behaviour happens regularly in Policy Gradient methods, especially in REINFORCE, due to high variance in gradient estimates, leading to high exploration rates. This phenomenon is referred to as *catastrophic forgetting*. It happens not only in RL but in sequential learning from artificial neural networks in general [47].

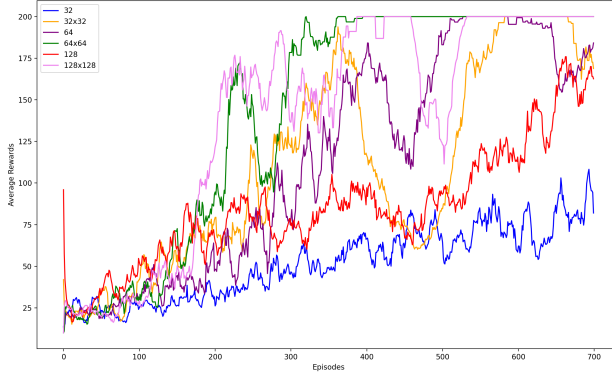


Figure 4: Classical ANN - CartPole-v0.

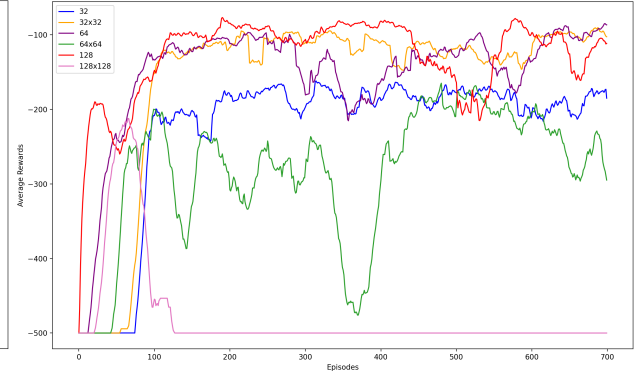


Figure 5: Classical ANN - Acrobot-v1.

The second step compares the performance of the quantum neural policy against the aforementioned classical architecture. Empirical evidence shows that increasing the number of layers would increase the expressivity of the model [48]. At the same time, increasing the number of layers leads to more complex optimization tasks, given that there are more parameters to be optimized. For some variational architectures, there is a threshold for the expressivity in terms of the number of layers [49]. We encountered precisely this in practice. For Cartpole the expressivity of the quantum neural policy saturates after three layers and for the Acrobot after five layers. The agent's performance is deteriorated rather than improved. The model hyperparameters, e.g. the learning rate, were fully tuned by trial and error as opposed to β that was randomly initialized. The optimal configuration of both the learning rate and the number of layers used in the quantum neural policy is present in table 2.

Environment	Learning rate	#Layers	Batch size
CartPole-v0	0.1	3	10
Acrobot-v1	0.1	5	10

Table 2: Hyperparameter configuration, the number of layers trained, and batch size for both environments.

Figures 6 and 7 compare the performance of the quantum and classical neural policies for the Cartpole and Acrobot environments, respectively. It is important to notice that the comparison was made by plotting the average cumulated reward through several episodes. Additionally, the benchmarking environments are noisy, therefore a running mean was computed to smooth the reward plots.

From Figure 6 we can conclude that the quantum neural policy outperforms its classical analogue in the CartPole-v0 environment. There is clear evidence that the quantum-inspired policy needs fewer interactions with the environment to converge to optimal behaviour. It is also clear that the quantum model exhibits higher variance than the classical one, which keeps the model from converging to a deterministic policy. Such stochastic policy always shows an exploration rate for suboptimal actions.

For the Acrobot-v1 environment, the quantum agent distinguishes itself from the classical one in terms of performance. It is perfectly observable that the Acrobot environment has a lower variance compared to the Cartpole. However, what is notable from Figure 7 is the lower variance of the quantum agent compared to its classical counterpart for the same environment.

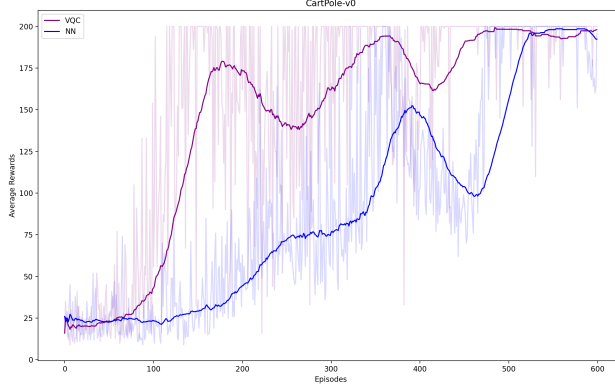


Figure 6: CartPole average cumulative reward.

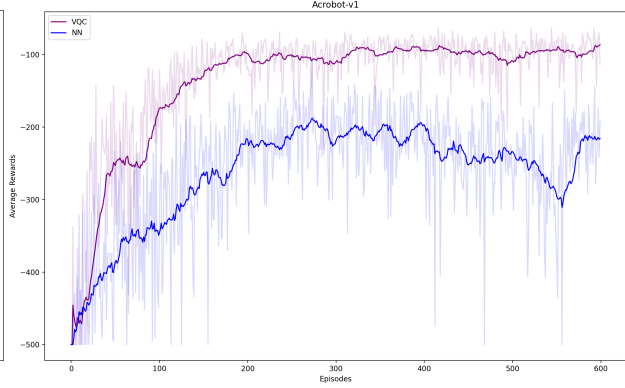


Figure 7: Acrobot average cumulative reward.

6.2 The effect of initialization

The parameters initialization strategy can dramatically improve the convergence of a machine learning algorithm. Initializing all weights to zero or some other constant makes the learning essentially prohibitive because all neurons will be computing the same function. Therefore, the only crucial property is that the initial parameters need to break the symmetry between different neurons [8]. Such is the reason for random initialization in practice. However, if the random parameters are too large, the activation function will always be saturated. That makes the learning task very difficult. For that reason, parameters are initialized at random but drawn from a Gaussian distribution. The He [50] and the Glorot [51] initialization strategies are the most commonly used to balance initialization and regularization [8].

In quantum machine learning models, the problem persists. However, in this section, we claim that the Glorot initialization can at least in principle be considered to initialize the parameters of quantum policy gradients very efficiently. The empirical results reported in Section 6.1 were obtained using such a strategy.

The Glorot strategy samples the parameters of the network from a normal distribution $\mathcal{N}(0, std^2)$ with standard deviation given by Equation (36):

$$std = gain * \sqrt{\frac{2}{fan_{in} + fan_{out}}} \quad (36)$$

where $gain$ is a constant multiplicative factor, fan_{in} is the number of inputs and fan_{out} the number of outputs. It was devised to initialize all layers with approximately the same activation and gradient variance. Furthermore, it works under the assumption that the neural network does not have any nonlinear activations, thus making it reducible to a chain of matrix multiplications. The latter assumption motivates the use of this strategy in quantum learning models, given that quantum neural networks are composed of unitary layers without nonlinearities. Essentially, the only nonlinearity is introduced by the measurement [38]. In the quantum setting, we considered that fan_{in} corresponds to the number of features embedded in the VQC and fan_{out} as the number of computational basis measurements.

Figures 8, 9 plot the average reward obtained by the quantum agent in the CartPole and Acrobot environments respectively, following the most common initialization strategies. It is fair to conclude that the Glorot initialization has the best performance and stability among the two.

7 Measuring Advantage

In this section further steps are taken towards studying possible advantages of quantum RL agents from a theoretical perspective, following two different strategies:

- **Parameter Count** - Comparison between quantum and classical agents in terms of the number of parameters trained. It is not yet clear whether this is a robust approach to quantify advantage, given that the number of parameters alone can be misleading. For example, the function $\sin(\theta)$ has a single parameter and it is more complex than polynomial $ax^3 + bx^2 + cx + d$. However, having smaller networks could enable solutions for larger problems at a smaller cost. Even though only parameter-shift rules are allowed on real quantum

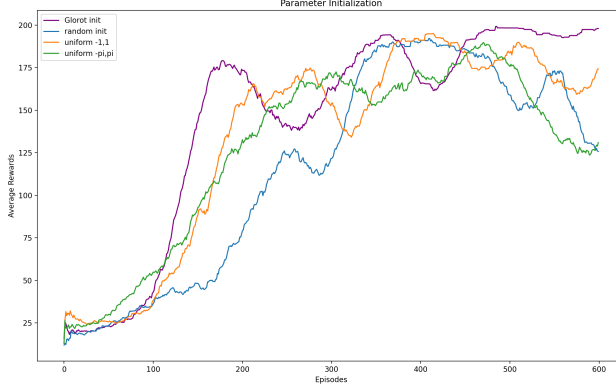


Figure 8: CartPole initializations.

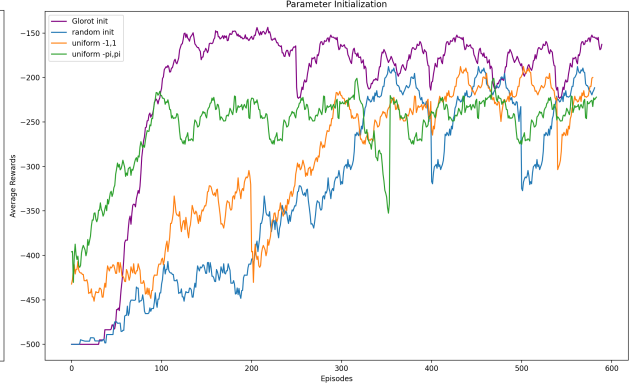


Figure 9: Acrobot initializations.

hardware, it enables a lower cost on memory than backpropagation. Perhaps for large enough problems, the training difference may be negligible from a tradeoff between memory and time consumption.

- **Fisher Information** - The spectrum of the Fisher Information matrix is related to the effect of barren plateaus in the optimization surface itself. Studying the properties of the matrix eigenvalues should help to explain the hardness of training.

7.1 Parameter Count

In this section we compare the number of optimized parameters in the quantum and classical neural policy for the simulated environments, summarized in Table 3. The input layer of a classical neural network is related to the number of qubits in a quantum circuit. Furthermore, we take the number of layers in the VQC as the number of hidden layers in a classical neural network. Given that the quantum circuit is unitary, the number of neurons in a quantum neural network is constant, i.e. equal to the system’s number of qubits.

Environment	Policy	Input layer	Output layer	Neurons	Rotations per qubit	β	#Parameters
CartPole-v0	Quantum	4	2	N.A	2	Yes	25
CartPole-v0	Classical	4	2	64	N.A	No	384
Acrobot-v1	Quantum	6	3	N.A	2	Yes	33
Acrobot-v1	Classical	6	3	64	N.A	No	576

Table 3: Number of parameters trained for both environments

Table 3 documents a massive reduction in the number of parameters in the quantum neural network when compared with the classical counterpart, for all three benchmarking environments. Notice that the comparison is between the quantum model and the best empirical classical model as depicted in Figure 4. In the CartPole environment, we obtained a reduction in the order of ~ 15 and a reduction of ~ 17 for the Acrobot environment.

7.2 Fisher Spectrum

The Fisher Information [52] is crucial both in computation and statistics as a measure of the amount of information in a random variable X in a statistical model parameterized by θ . In its most general form it amounts to the covariance matrix of the gradient vectors, or score functions. Having data points x described by the model $p(x|\theta)$ where $\theta \in \mathbb{R}^k$ and x is drawn i.i.d from p , the Fisher Information matrix

$$F(\theta) = \mathbb{E}_{x \sim p} [\nabla_{\theta} \log p(x|\theta) \nabla_{\theta} \log p(x|\theta)^{\top}] \in \mathbb{R}^{k \times k} \quad (37)$$

captures the sensitivity with respect to changes in the parameter space. It can be approximated by the empirical Fisher information matrix as in Equation (38):

$$F(\theta) = \frac{1}{T} \sum_{i=1}^T \nabla_{\theta} \log p(x_i | \theta) \nabla_{\theta} \log p(x_i | \theta)^{\top} \quad (38)$$

Equation (38) captures the curvature of the score function at all parameter combinations. That is, it can be used as a measure for the study of barren plateaus in maximum likelihood estimators [53], given that all the entries of the matrix will approach zero with the flatness of the model’s landscape. This effect is captured by looking at the spectrum of the matrix. If the model is in a barren plateau, then the eigenvalues of the matrix will be closer to zero [54].

In the context of policy gradients, the empirical Fisher information matrix [55] is obtained by multiplying the vector resultant of the gradient of the log-policy with its transpose as in Equation (39):

$$F(\theta) = \frac{1}{T} \sum_{t=1}^T \nabla_{\theta} \log \pi(a_t | s_t, \theta) \nabla_{\theta} \log \pi(a_t | s_t, \theta)^{\top} \quad (39)$$

Inspecting the spectrum of the matrix in Equation (39) reveals the flatness of the loss landscape. Thus, it can be used to harness the hardness of the model’s trainability for both RL agents based on classical neural networks and VQC’s [54].

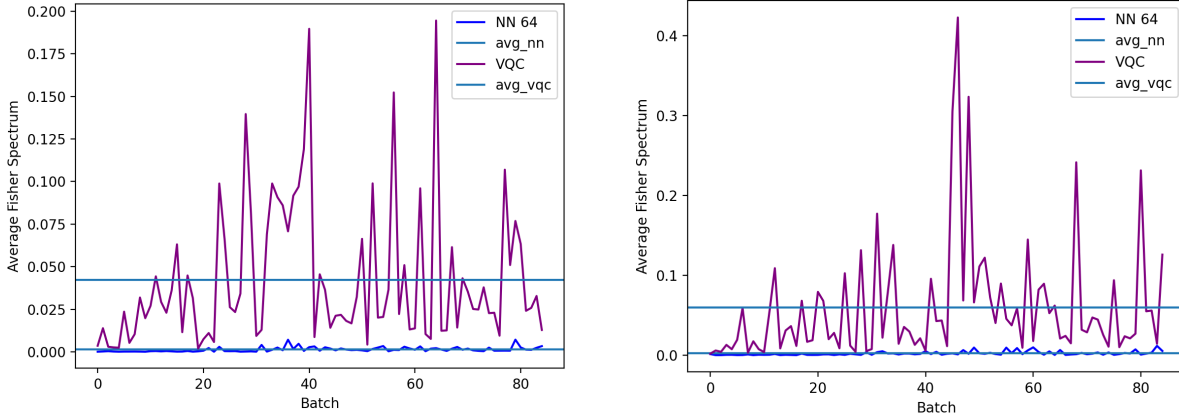


Figure 10: Fisher spectrum for the CartPole environment. Figure 11: Fisher spectrum for the Acrobot environment.

Figures 10 and 11 plot the average Fisher information spectrum for the respective batch size used in training epochs during the entire training for the CartPole and Acrobot environments, respectively. The spectrum of the Fisher information matrix of the quantum model exhibits significant larger eigenvalues than the classical model on average during the entire training. We observe the same behaviour for both CartPole and Acrobot environments. This explains the improvement of the training performance for quantum agents (section 6) compared to classical ones. Furthermore, the spectrum of the quantum agent in the Acrobot environment is larger, on average, than the spectrum of the quantum agent in the CartPole environment, which may explain the observed stability in training in the Acrobot compared to CartPole. Although the empirical evidence seems encouraging, further analysis is required to completely understand the behavior of both the classical and quantum agents.

8 Quantum control

In Section 6 we validated the performance of the quantum variational agent in well-known benchmarking environments. However, such environments are classical, i.e. they exhibit a trade of information between a quantum and a classical channel. Such trade incurs an overhead in the quantum system relative to the encoding of classical information into the quantum processor. In complex real-world problems, efficient encoding of information constitute the bottleneck of NISQ devices, and a poor encoding scheme may reduce the potential quantum advantage [36]. However, if the quantum agent works within a quantum environment, the cost of data encoding can often be neglected, and there is room for potential quantum advantages from quantum data [56]. To that end, in this section, we design a quantum environment as

a use case for the variational quantum model constructed in Section 4. This environment constitutes a quantum control problem, namely quantum state preparation. In this setting, the quantum agent must learn how to prepare the state $|1\rangle$ with high fidelity, starting from ground state $|0\rangle$. The mapping $|0\rangle \mapsto |1\rangle$ can be characterized by a time-dependent Hamiltonian $H(t)$ of the form of Equation (40) as described in [57].

$$H(t) = 4J(t)\sigma_z + h\sigma_x \quad (40)$$

where h represents the single-qubit energy gap between tunable control fields. In this work, h is considered a constant energy unit. $J(t)$ represents the dynamical pulses controlled by the RL quantum agent. In a model-free setting, the RL agent controls the pulse sequence, and the quantum environment prepares the state associated with time step $t+1$, given the Hamiltonian at time step t . The fidelity between the target state $|\psi_T\rangle = |1\rangle$ and the prepared state $|\psi_t\rangle$ naturally serves as the reward r_t for the agent at time step t , as in Equation (41).

$$r_t = |\langle \psi_t | \psi_T \rangle|^2 \quad (41)$$

The goal is, thus, using the policy gradient algorithm of Section 4 to learn how to maximize reward, i.e. to maximize the fidelity. The full RL loop can be visualized in Figure 12.

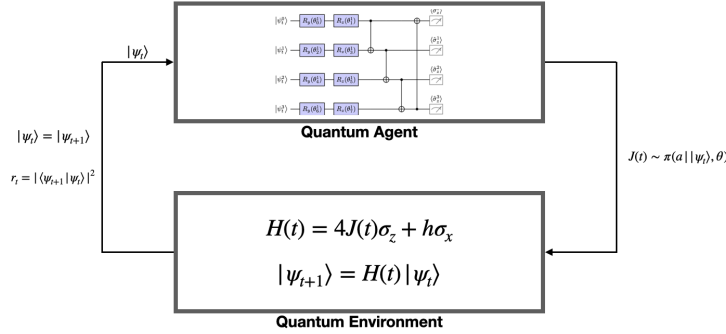


Figure 12: Agent-Environment interface for quantum control.

The learning procedure defines a fixed number of time steps $N = 20$, from which the RL agent must be able to create the desired quantum state. At each time step, the quantum environment prepares the quantum state obtained from applying the time-dependent Hamiltonian $H(t)$, converted to a set of unitary gates $U(t)$, such that

$$|\psi_{t+1}\rangle = U(t)|\psi\rangle \quad (42)$$

Each sequence of N pulses corresponds to an episode. The quantum agent should learn the optimal behaviour, i.e. the optimal pulse sequence, such that it corresponds to the state with maximum fidelity throughout several episodes. The quantum variational architecture selected to solve the quantum control environment was the same as described in Section 4. In this setting, the main difference is the lack of encoding. The quantum agent receives the quantum state obtained from the corresponding time-step Hamiltonian applied at each time step. The number of actions in this setting is only two, $A = [0, 1]$, representing the binary behaviour of the agent, i.e. if decides to apply a pulse $A = 1$, or not $A = 0$. A sequence of N actions corresponds to N pulses. Figure 13 illustrates the running average reward evolution through a sequence of 2000 episodes (dark-purple) and the full noisy rewards (light-purple). The running average converges to the maximum fidelity. One can easily conclude that the agent learns how to produce the desired state with maximum fidelity.

The learning curve plotted in Figure 13 was obtained following a policy generated from the variational quantum architecture suggested in Section 4. In this case, a single parameterized layer was enough to produce high fidelity results. Figure 14 represents the average spectrum of the Fisher Information matrix for the quantum control experiment.

It can be observed in Figure 14 that the eigenvalues of the Fisher information matrix decrease during the training, becoming null at approximately half of the training. At first, the plot can be misleading because it indicates the presence of barren plateaus. However, Figure 13 shows that the training converged to the optimal fidelity state, i.e. the training parameters already converged to the loss function global maximum and thus, the gradients should become null. In this case, the flatness of the loss function does not correspond to barren plateaus and, thus to the infeasibility of training but rather signals the convergence to the maximum.

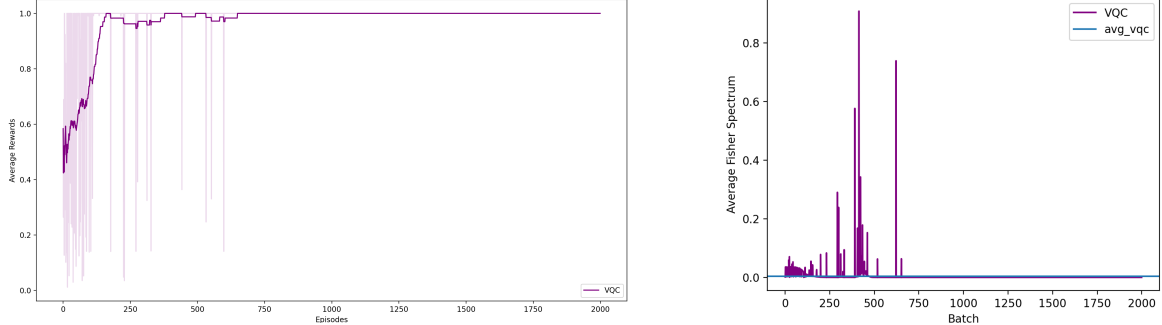


Figure 13: Final reward obtained at each episode corresponding to the fidelity of the quantum state prepared. Figure 14: Average Fisher spectrum for the quantum control problem.

In the setting of quantum control (at least in this small experience), the Glorot initialization technique (see Section 6.2) appears superior with respect to other random initialization strategies. That is, initializing the parameters of the variational quantum circuit with the Glorot strategy leads to faster convergence towards the maximum fidelity state and stable training curves. Such behaviour can be observed in Figure 15.

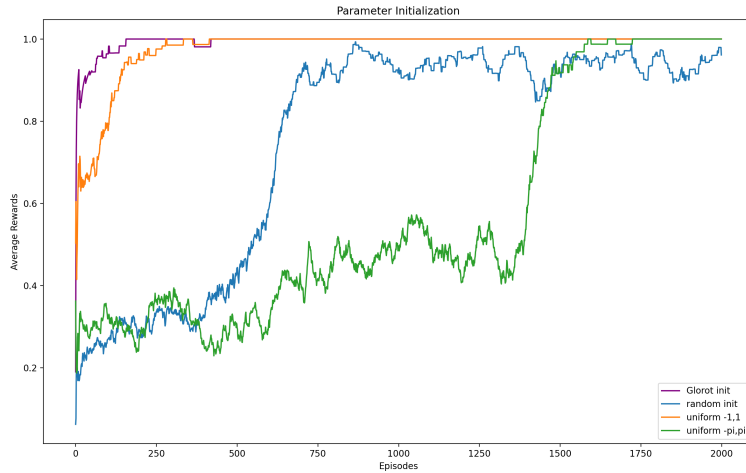


Figure 15: Different random initialization strategies applied to the quantum control problem.

9 Conclusions

In this work, we embed a VQC into the decision-making process of a RL agent, following the policy gradient algorithm. This resulted in a simpler variational architecture that was used to effectively solve well-known benchmarking environments. The empirical results demonstrate that such variational quantum models outperform classical neural networks in a selection of benchmarking environments. In particular, it shows that the quantum-inspired policy needs fewer interactions to converge to an optimal behaviour. Moreover, the quantum model benefit from a reduction in terms of the number of parameters that need to be optimized.

The same quantum model was used for both computing expectation values and estimating the gradients following parameter-shift rules. A bound on the number of samples required to estimate an ϵ -approximation of the gradient using parameter-shift rules was demonstrated: we proved that the sample complexity grows only logarithmically with the number of parameters, taking into account the number repetitions of the quantum circuit.

A first step is taken towards investigating the effect of barren plateaus in quantum policy gradients by exploiting the spectrum of the Fisher Information matrix. For benchmarking environments, the Fisher spectrum of the quantum models seems to be composed of larger eigenvalues when compared to the classical counterpart. In principle, this suggests that the optimization surface is less prone to plateaus in these cases. The latter observation reinforces the empirical advantage observed in the quantum model. Furthermore, the variational quantum model was applied to the

problem of quantum control, namely quantum state preparation. It was verified that a quantum model with a single layer is able to prepare a single-qubit at state $|1\rangle$ with high fidelity.

With respect to future work, in the light of the empirical results shown for the benchmarking environments, it would be interesting to apply such RL-based variational quantum models to quantum control problems of large dimension. Specifically, their application to noisy environments, would be of great general interest. It is also crucial to study the effect of the quantum models from a theoretical basis. The quantum Fisher Information [58] should be addressed to analyze the information behind these quantum states. Moreover, it would be interesting to embed the Quantum Fisher Information in a Natural Gradient optimization [59] to derive Quantum Natural Policy Gradients. Advanced RL models such as Actor-Critic or Deep Deterministic Policy Gradients (DDPG), could be enhanced by this sort of quantum-aware optimization.

References

- [1] David Silver, Aja Huang, Chris J. Maddison, Arthur Guez, L. Sifre, George van den Driessche, Julian Schrittwieser, Ioannis Antonoglou, Vedavyas Panneershelvam, Marc Lanctot, Sander Dieleman, Dominik Grewe, John Nham, Nal Kalchbrenner, Ilya Sutskever, Timothy P. Lillicrap, Madeleine Leach, Koray Kavukcuoglu, Thore Graepel, and Demis Hassabis. Mastering the game of go with deep neural networks and tree search. *Nature*, 529:484–489, 2016.
- [2] Julian Schrittwieser, Ioannis Antonoglou, Thomas Hubert, Karen Simonyan, Laurent Sifre, Simon Schmitt, Arthur Guez, Edward Lockhart, Demis Hassabis, Thore Graepel, and et al. Mastering atari, go, chess and shogi by planning with a learned model. *Nature*, 588(7839):604–609, Dec 2020. ISSN 1476-4687. doi:10.1038/s41586-020-03051-4. URL <http://dx.doi.org/10.1038/s41586-020-03051-4>.
- [3] B Ravi Kiran, Ibrahim Sobh, Victor Talpaert, Patrick Mannion, Ahmad A. Al Sallab, Senthil Yogamani, and Patrick Pérez. Deep reinforcement learning for autonomous driving: A survey, 2021.
- [4] Xiao-Yang Liu, Hongyang Yang, Qian Chen, Runjia Zhang, Liuqing Yang, Bowen Xiao, and Christina Dan Wang. Finrl: A deep reinforcement learning library for automated stock trading in quantitative finance, 2020.
- [5] Amir Mosavi, Pedram Ghamisi, Yaser Faghan, Puhong Duan, and Shahab Shamshirband. Comprehensive review of deep reinforcement learning methods and applications in economics. Mar 2020. doi:10.20944/preprints202003.0309.v1. URL <http://dx.doi.org/10.20944/preprints202003.0309.v1>.
- [6] M. Mehdi Afsar, Trafford Crump, and Behrouz Far. Reinforcement learning based recommender systems: A survey, 2021.
- [7] Mogens Dalgaard, Felix Motzoi, Jens Jakob Sørensen, and Jacob Sherson. Global optimization of quantum dynamics with alphazero deep exploration. *npj Quantum Information*, 6(1), Jan 2020. ISSN 2056-6387. doi:10.1038/s41534-019-0241-0. URL <http://dx.doi.org/10.1038/s41534-019-0241-0>.
- [8] Ian Goodfellow, Yoshua Bengio, and Aaron Courville. *Deep Learning*. The MIT Press, 2016. ISBN 0262035618.
- [9] Vedran Dunjko, Jacob M. Taylor, and Hans J. Briegel. Quantum-Enhanced Machine Learning. *Physical Review Letters*, 117(13):1–19, 2016. ISSN 10797114. doi:10.1103/PhysRevLett.117.130501.
- [10] Vedran Dunjko, Yi-Kai Liu, Xingyao Wu, and Jacob M. Taylor. Exponential improvements for quantum-accessible reinforcement learning. 2017. URL <http://arxiv.org/abs/1710.11160>.
- [11] Giuseppe Davide Paparo, Vedran Dunjko, Adi Makmal, Miguel Angel Martin-Delgado, and Hans J. Briegel. Quantum speedup for active learning agents. *Physical Review X*, 4(3):1–14, 2014. ISSN 21603308. doi:10.1103/PhysRevX.4.031002.
- [12] André Sequeira, Luis Paulo Santos, and Luis Soares Barbosa. Quantum tree-based planning. *IEEE Access*, 9: 125416–125427, 2021. doi:10.1109/ACCESS.2021.3110652.
- [13] Vedran Dunjko and Hans J Briegel. Machine learning & artificial intelligence in the quantum domain: a review of recent progress. *Reports on Progress in Physics*, 81(7):074001, jun 2018. doi:10.1088/1361-6633/aab406. URL <https://doi.org/10.1088/1361-6633/aab406>.
- [14] V. Saggio, B. E. Asenbeck, A. Hamann, T. Strömberg, P. Schiansky, V. Dunjko, N. Friis, N. C. Harris, M. Hochberg, D. Englund, and et al. Experimental quantum speed-up in reinforcement learning agents. *Nature*, 591(7849): 229–233, Mar 2021. ISSN 1476-4687. doi:10.1038/s41586-021-03242-7. URL <http://dx.doi.org/10.1038/s41586-021-03242-7>.
- [15] Richard S. Sutton and Andrew G. Barto. *Reinforcement Learning: An Introduction*. A Bradford Book, Cambridge, MA, USA, 2018. ISBN 0262039249.

[16] John Preskill. Fault-tolerant quantum computation. *arXiv: Quantum Physics*, 1997.

[17] John Preskill. Quantum computing in the nisq era and beyond. *Quantum*, 2:79, Aug 2018. ISSN 2521-327X. doi:10.22331/q-2018-08-06-79. URL <http://dx.doi.org/10.22331/q-2018-08-06-79>.

[18] Edward Farhi and Hartmut Neven. Classification with quantum neural networks on near term processors, 2018.

[19] Maria Schuld, Ryan Sweke, and Johannes Jakob Meyer. Effect of data encoding on the expressive power of variational quantum-machine-learning models. *Physical Review A*, 103(3), Mar 2021. ISSN 2469-9934. doi:10.1103/physreva.103.032430. URL <http://dx.doi.org/10.1103/PhysRevA.103.032430>.

[20] Ronald J. Williams. Simple statistical gradient-following algorithms for connectionist reinforcement learning. *Machine Learning*, 8:229–256, 2004.

[21] M.R. James. Optimal quantum control theory. *Annual Review of Control, Robotics, and Autonomous Systems*, 4(1):343–367, 2021. doi:10.1146/annurev-control-061520-010444. URL <https://doi.org/10.1146/annurev-control-061520-010444>.

[22] José Martín-Guerrero and Lucas Lamata. Reinforcement learning and physics. *Applied Sciences*, 11:8589, 09 2021. doi:10.3390/app11188589.

[23] Samuel Yen Chi Chen, Chao Han Huck Yang, Jun Qi, Pin Yu Chen, Xiaoli Ma, and Hsi Sheng Goan. Variational Quantum Circuits for Deep Reinforcement Learning. *IEEE Access*, 2020. ISSN 21693536. doi:10.1109/ACCESS.2020.3010470.

[24] Owen Lockwood and Mei Si. Reinforcement learning with quantum variational circuits. In *Proceedings of the 16th AAAI Conference on Artificial Intelligence and Interactive Digital Entertainment, AIIDE 2020*, 2020. ISBN 9781577358497.

[25] Owen Lockwood and Mei Si. Playing atari with hybrid quantum-classical reinforcement learning. 2021.

[26] Sofiene Jerbi, Casper Gyurik, Simon Marshall, Hans J. Briegel, and Vedran Dunjko. Variational quantum policies for reinforcement learning, 2021.

[27] Fabio Sanches, Sean Weinberg, Takanori Ide, and Kazumitsu Kamiya. Short quantum circuits in reinforcement learning policies for the vehicle routing problem, 2021.

[28] Shaojun Wu, Shan Jin, Dingding Wen, and Xiaoting Wang. Quantum reinforcement learning in continuous action space, 2021.

[29] Esma Aimeur, Gilles Brassard, and Sébastien Gambs. Machine learning in a quantum world. In Luc Lamontagne and Mario Marchand, editors, *Advances in Artificial Intelligence*, pages 431–442, Berlin, Heidelberg, 2006. Springer Berlin Heidelberg. ISBN 978-3-540-34630-2.

[30] Alekh Agarwal, Nan Jiang, and S. Kakade. Reinforcement learning: Theory and algorithms. 2019.

[31] R. Sutton, David A. McAllester, Satinder Singh, and Y. Mansour. Policy gradient methods for reinforcement learning with function approximation. In *NIPS*, 1999.

[32] Evan Greensmith, Peter L. Bartlett, and Jonathan Baxter. Variance reduction techniques for gradient estimates in reinforcement learning. *J. Mach. Learn. Res.*, 5:1471–1530, December 2004. ISSN 1532-4435.

[33] V. Konda and J. Tsitsiklis. Actor-critic algorithms. In *NIPS*, 1999.

[34] Kishor Bharti, Alba Cervera-Lierta, Thi Ha Kyaw, Tobias Haug, Sumner Alperin-Lea, Abhinav Anand, Matthias Degroote, Hermanni Heimonen, Jakob S. Kottmann, Tim Menke, Wai-Keong Mok, Sukin Sim, Leong-Chuan Kwek, and Alán Aspuru-Guzik. Noisy intermediate-scale quantum (nisq) algorithms, 2021.

[35] Maria Schuld and Francesco Petruccione. *Supervised Learning with Quantum Computers*. Springer Publishing Company, Incorporated, 1st edition, 2018. ISBN 3319964232.

[36] Ryan LaRose and Brian Coyle. Robust data encodings for quantum classifiers. *ArXiv*, abs/2003.01695, 2020.

[37] M. Cerezo, Andrew Arrasmith, Ryan Babbush, Simon C. Benjamin, Suguru Endo, Keisuke Fujii, Jarrod R. McClean, Kosuke Mitarai, Xiao Yuan, Lukasz Cincio, and Patrick J. Coles. Variational quantum algorithms. *Nature Reviews Physics*, 3(9):625–644, 2021. doi:10.1038/s42254-021-00348-9. URL <https://doi.org/10.1038/s42254-021-00348-9>.

[38] Michael A. Nielsen and Isaac L. Chuang. *Quantum Computation and Quantum Information: 10th Anniversary Edition*. Cambridge University Press, USA, 10th edition, 2011. ISBN 1107002176.

[39] Mateusz Ostaszewski, Edward Grant, and Marcello Benedetti. Structure optimization for parameterized quantum circuits. *Quantum*, 5:391, Jan 2021. ISSN 2521-327X. doi:10.22331/q-2021-01-28-391. URL <http://dx.doi.org/10.22331/q-2021-01-28-391>.

[40] Ryan Sweke, Frederik Wilde, Johannes Meyer, Maria Schuld, Paul K. Faehrmann, Barthélémy Meynard-Piganeau, and Jens Eisert. Stochastic gradient descent for hybrid quantum-classical optimization. *Quantum*, 4: 314, Aug 2020. ISSN 2521-327X. doi:10.22331/q-2020-08-31-314. URL <http://dx.doi.org/10.22331/q-2020-08-31-314>.

[41] Maria Schuld, Ville Bergholm, Christian Gogolin, Josh A. Izaac, and Nathan Killoran. Evaluating analytic gradients on quantum hardware. *Physical Review A*, 99:032331, 2019.

[42] Wassily Hoeffding. Probability inequalities for sums of bounded random variables. *Journal of the American Statistical Association*, 58(301):13–30, 1963. doi:10.1080/01621459.1963.10500830. URL <https://www.tandfonline.com/doi/abs/10.1080/01621459.1963.10500830>.

[43] Greg Brockman, Vicki Cheung, Ludwig Pettersson, Jonas Schneider, John Schulman, Jie Tang, and Wojciech Zaremba. Openai gym, 2016.

[44] Ville Bergholm, Josh Izaac, Maria Schuld, Christian Gogolin, M. Sohaib Alam, Shahnaz Ahmed, Juan Miguel Arrazola, Carsten Blank, Alain Delgado, Soran Jahangiri, Keri McKiernan, Johannes Jakob Meyer, Zeyue Niu, Antal Száva, and Nathan Killoran. PennyLane: Automatic differentiation of hybrid quantum-classical computations, 2020.

[45] Adam Paszke, Sam Gross, Soumith Chintala, Gregory Chanan, Edward Yang, Zachary DeVito, Zeming Lin, Alban Desmaison, Luca Antiga, and Adam Lerer. Automatic differentiation in pytorch. 2017.

[46] Diederik P. Kingma and Jimmy Ba. Adam: A method for stochastic optimization, 2017.

[47] Michael McCloskey and Neal J. Cohen. Catastrophic interference in connectionist networks: The sequential learning problem. volume 24 of *Psychology of Learning and Motivation*, pages 109–165. Academic Press, 1989. doi:[https://doi.org/10.1016/S0079-7421\(08\)60536-8](https://doi.org/10.1016/S0079-7421(08)60536-8). URL <https://www.sciencedirect.com/science/article/pii/S0079742108605368>.

[48] Maria Schuld. Quantum machine learning models are kernel methods. 2021.

[49] Sukin Sim, Peter D. Johnson, and Alán Aspuru-Guzik. Expressibility and entangling capability of parameterized quantum circuits for hybrid quantum-classical algorithms. *Advanced Quantum Technologies*, 2(12):1900070, Oct 2019. ISSN 2511-9044. doi:10.1002/qute.201900070. URL <http://dx.doi.org/10.1002/qute.201900070>.

[50] Kaiming He, X. Zhang, Shaoqing Ren, and Jian Sun. Delving deep into rectifiers: Surpassing human-level performance on imagenet classification. *2015 IEEE International Conference on Computer Vision (ICCV)*, pages 1026–1034, 2015.

[51] Xavier Glorot and Yoshua Bengio. Understanding the difficulty of training deep feedforward neural networks. In *AISTATS*, 2010.

[52] Alexander Ly, Maarten Marsman, Josine Verhagen, Raoul Grasman, and Eric-Jan Wagenmakers. A tutorial on fisher information, 2017.

[53] Ryo Karakida, Shotaro Akaho, and Shun ichi Amari. Universal statistics of fisher information in deep neural networks: Mean field approach, 2019.

[54] Amira Abbas, David Sutter, Christa Zoufal, Aurelien Lucchi, Alessio Figalli, and Stefan Woerner. The power of quantum neural networks. *Nature Computational Science*, 1(6):403–409, Jun 2021. ISSN 2662-8457. doi:10.1038/s43588-021-00084-1. URL <http://dx.doi.org/10.1038/s43588-021-00084-1>.

[55] Sham Kakade. A natural policy gradient. In *Proceedings of the 14th International Conference on Neural Information Processing Systems: Natural and Synthetic*, NIPS’01, page 1531–1538, Cambridge, MA, USA, 2001. MIT Press.

[56] Hsin-Yuan Huang, Michael Broughton, M. Mohseni, Ryan Babbush, Sergio Boixo, Hartmut Neven, and Jarrod McClean. Power of data in quantum machine learning. *Nature Communications*, 12, 05 2021. doi:10.1038/s41467-021-22539-9.

[57] Xiao-Ming Zhang, Zezhu Wei, Raza Asad, Xu-Chen Yang, and Xin Wang. When does reinforcement learning stand out in quantum control? a comparative study on state preparation. *npj Quantum Information*, 5:1–7, 10 2019. doi:10.1038/s41534-019-0201-8.

[58] Johannes Jakob Meyer. Fisher information in noisy intermediate-scale quantum applications. *Quantum*, 5: 539, Sep 2021. ISSN 2521-327X. doi:10.22331/q-2021-09-09-539. URL <http://dx.doi.org/10.22331/q-2021-09-09-539>.

[59] James Stokes, Josh Izaac, Nathan Killoran, and Giuseppe Carleo. Quantum natural gradient. *Quantum*, 4: 269, May 2020. ISSN 2521-327X. doi:10.22331/q-2020-05-25-269. URL <http://dx.doi.org/10.22331/q-2020-05-25-269>.